Journal of Electronic Materials (2024) 53:4997–5006
https://doi.org/10.1007/s11664-024-11086-w

28TH INTERNATIONAL CONFERENCE ON NUCLEAR TRACKS AND RADIATION MEASUREMENTS

Modeling of ZrS_2/MoS_2 Heterostructures for Photovoltaic Applications

Shubhra Gupta[1] · Gayatri Shishodia[2] · P. K. Shishodia[1]

Received: 19 January 2024 / Accepted: 27 March 2024 / Published online: 20 April 2024

Abstract
A single-junction heterostructure based on transition metal chalcogenides has been modeled using a solar cell capacitance simulator (SCAPS) to explore non-toxic materials for solar cell applications. The performance parameters of the proposed AZO/ZrS_2/MoS_2 heterojunction have been analyzed by varying the thickness of each layer and the doping concentrations. The impact of defect densities in ZrS_2 and MoS_2 on the performance parameters has been studied. The influence of metal back contact on the parameters has also been explored. The highest power conversion efficiency (PCE) of 14.13% has been obtained for thicknesses of 0.1 μm, 0.2 μm, and 3.0 μm of AZO, ZrS_2 , and MoS_2 layers, respectively. Other parameters obtained were the open circuit voltage (V_{oc}) = 0.5707 V, short circuit current density (J_{sc}) = 34.02 mA/cm^3 , and fill factor (FF) = 71.35%. The external quantum efficiency (EQE) response and J–V characteristics of the optimized junctions are presented. The exponential grading law in SCAPS for the graded MoS_2 layer has been implemented to further enhance the PCE. Solar cell efficiency improved from 14.13% to 21.14% on the selenization of the MoS_2 absorber layer.

Keywords SCAPS · transition metal chalcogenide · power conversion efficiency · grading law · selenization

Introduction

During the last few years, the quasi-2D characteristics of transition metal chalcogenides (TMCs) have attracted a lot of attention of researchers for their unique properties, and have been actively investigated for their widespread applications in optoelectronic and photonic devices.[1–7] Earth-abundant constituent elements, non-toxic nature, high absorption coefficient, superior mobility, and a chemically stable and layered crystal structure are some of the exciting properties that make transition materials most appropriate for different device applications, such as photovoltaics,[8–11] photodetectors,[12–17] field effect devices,[18–20] light emitting diodes,[21,22] etc. TMCs also demonstrate a tunable band structure, beneficial for achieving desirable characteristics on strain engineering, doping, and layer stacking.[23]

Cadmium-based II–VI compounds have been explored as solar cell materials for their effective photon-to-electric conversion efficiencies. However, the toxic nature of Cd has compelled the finding of alternatives suitable for photovoltaic applications. In this paper, an attempt has been made to study the solar cell characteristics of heterojunctions formed between two TMCs, namely zirconium disulfide (ZrS_2) and molybdenum disulfide (MoS_2).

The Schottky junction formed between a ZrS_2 nanobelt network and an Au metal contact showed a solar cell response for interesting applications in nanostructured optoelectronic devices.[9] A high-performance efficiency (9.72%) of the ZrS_2/CZTS structure has been computed using a solar cell capacitance simulator (SCAPS) against a Cd-free buffer layer.[8] The selenization of CZTS further improves the efficiency, as demonstrated by Gupta et al. using the exponential grading law in SCAPS[24]. Ultrathin sheets of MoS_2 can act as efficient transparent conducting n-type electrodes in silicon heterostructure solar cells, as presented in the simulation study by Chaudhary et al. [25] A maximum efficiency of 16.4% has been evaluated using AFORS-HET software after optimization. A thin layer of MoS_2 has been demonstrated as an electron transport layer in perovskite solar cells, and the fabricated device exhibited a high power conversion efficiency

✉ P. K. Shishodia
pkshishodia@zh.du.ac.in

[1] Department of Electronics, Zakir Husain Delhi College, University of Delhi, Delhi 110002, India

[2] Department of Physics, Zakir Husain Delhi College, University of Delhi, Delhi 110002, India

of 13.1% due to its fascinating optical and electrical properties.[26] Other than single-junction solar structures, a tandem solar cell based on ZrS_2-MoS_2 has been numerically simulated to obtain current matching conditions at 0.267 μm and 0.2 μm thicknesses of ZrS_2 and MoS_2 , respectively.[27]

In the present simulations, a heterojunction formed between ZrS_2 and MoS_2 thin films has been investigated using SCAPS for solar cell characteristics. An AZO/ZrS_2 / MoS_2 structure has been modeled and optimized by varying the physical and geometrical parameters of each layer. Solar cell performance parameters, such as efficiency, open circuit voltage, short circuit current density, and fill factor (FF), have been examined by varying the layer thicknesses and doping concentrations. Comprehensive investigations have been undertaken by considering different materials, i.e., platinum (Pt), nickel (Ni), and gold (Au) for back contact. The external quantum efficiency (EQE) and *J–V* characteristics are presented for the optimized structure. Additionally, the variation of sulphur-selenium concentration in MoS_2 layer has been examined numerically using the exponential grading law.

Device Structure and Numerical Simulations

Analytical modeling of the AZO/ZrS_2/MoS_2 heterostructure was implemented on the SCAPS software, which is a one-dimensional simulation tool designed specifically to numerically analyze thin-film solar cells.[28] Interpretation of solar cell parameters using SCAPS is based on solving the Poisson's and continuity equations[29,30:]

$$\frac{d^2}{dx^2}\Psi(x) = \frac{q}{\varepsilon_0\varepsilon_r}\left(p(x) - n(x) + N_D - N_A + \rho_p - \rho_n\right) \quad (1)$$

where $\Psi(x)$ is the electrostatic potential, q is the electrical charge, ε_r is relative, ε_0 is the vacuum permittivity, p and n are the hole and electron concentrations, respectively, N_D is donor impurities, N_A is acceptor type, and ρ_p and ρ_n are hole and electron distributions, respectively.

$$\frac{d}{dx}J_n(x) - q\frac{\partial n(x)}{\partial t} - q\frac{\partial \rho_n}{\partial t} = G(x) - R(x) \quad (2)$$

$$\frac{d}{dx}J_p(x) - q\frac{\partial p(x)}{\partial t} + q\frac{\partial \rho_n}{\partial t} = G(x) - R(x) \quad (3)$$

where J_n and J_p are electron and hole current densities, respectively, and $G(x)$ and $R(x)$ are charge generation and recombination rates, respectively.

In the SCAPS program, it is feasible to define solar cells with up to seven layers that exclude front and back contacts. Simulation is performed at room temperature and under AM1.5 solar irradiation conditions. To define the solar cell geometry, different material parameters can be specified separately for each layer. For the modeled solar cell as shown in Fig. 1, material parameters such as thickness, band gap, permittivity, electron and hole mobility, effective density of states, defects, etc. have been defined for the respective layers, AZO, ZrS_2 , and MoS_2. The parameters to perform the simulations are defined in Table I and taken from the reported literature.

Results and Discussion

The effect of the geometrical and physical parameters of different layers have been studied to characterize the performance of the proposed heterostructure. Solar cell efficiency, open circuit voltage, current density, and FF have been computed for the variation of layer thickness versus doping concentration. Also, the effect of the variation of defect density in the ZrS_2 and MoS_2 layers on solar cell performance has been considered. The *J–V* characteristics and external

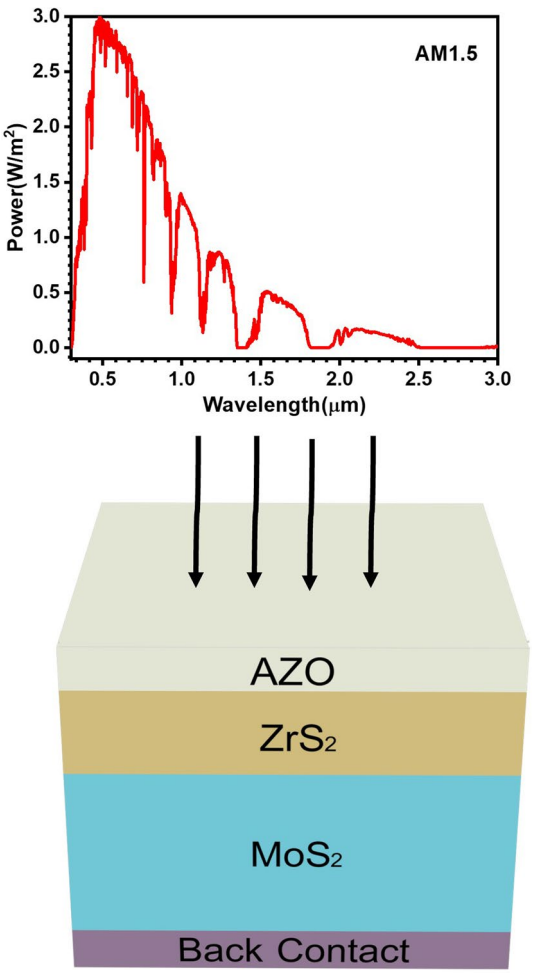

Fig. 1 Solar cell device model.

Table I Physical and opto-electrical parameters for different layers[24, 31]

Layer properties	ZrS_2	MoS_2	Al-ZnO
Thickness, μm	0.1–0.3	1.0–5.0	0.1–0.3
Band gap, eV	1.7	1.29	3.3
Electron affinity	4.95	4.43	4.5
Relative permittivity	1.5–10.5	18	9
N_c, cm^{-3}	2.20E + 18	2.20E + 18	2.20E + 18
N_v, cm^{-3}	1.80E + 19	1.80E + 19	1.80E + 19
Thermal velocity of electron, cm/s	1.00E + 07	1.00E + 07	1.00E + 07
Thermal velocity of hole, cm/s	1.00E + 07	1.00E + 07	1.00E + 07
Electron mobility, cm^2/Vs	1250	400	200
Hole mobility, cm^2/Vs	695.8	8.5	5 to 50
Electron effective mass	1.62/0.31 mo	0.07 mo	0.24 mo
Hole effective mass	0.71 mo	0.09 mo	0.59 mo
N_d	1.00E + 19	1.00E + 10	1.00E + 19
N_a	1.00E + 10	1.00E + 18	1.00E + 10

quantum efficiency (EQE) response for the optimized layer thicknesses have been plotted. An increase in the efficiency by selenization of the absorber layer has also been observed using the exponential grading law in SCAPS.

Effect of Varying Layer Thicknesses and Doping Concentration

Photovoltaic parameters for the variation of AZO thickness and doping concentration have been computed and the contour plots are shown in Fig. 2. AZO thickness was varied in the range 0.1-0.3 μm and donor concentration in the range 1×10^{15}–$1 \times 10^{21} cm^{-3}$. It is noted that, as the thickness increases, the power conversion efficiency (PCE) and J_{sc} also improve for a constant dopant concentration, as shown in Fig. 2. The increase in conversion efficiency with thickness increases up to the donor concentration of $1 \times 10^{17} cm^{-3}$. For instance, the efficiency increases from 12.78% to 14.43% when the thickness increases from 0.1 μm to 0.3 μm for the doping concentration of $1 \times 10^{15} cm^{-3}$, and J_{sc} changes from 32.0 $mAcm^{-2}$ to 36.33 $mAcm^{-2}$ under similar conditions. However, the lowest efficiency and current density of 10.78% and 26.82 $mAcm^{-2}$ have been obtained for the $1 \times 10^{21} cm^{-3}$ doping level and 0.3-μm AZO layer thickness.

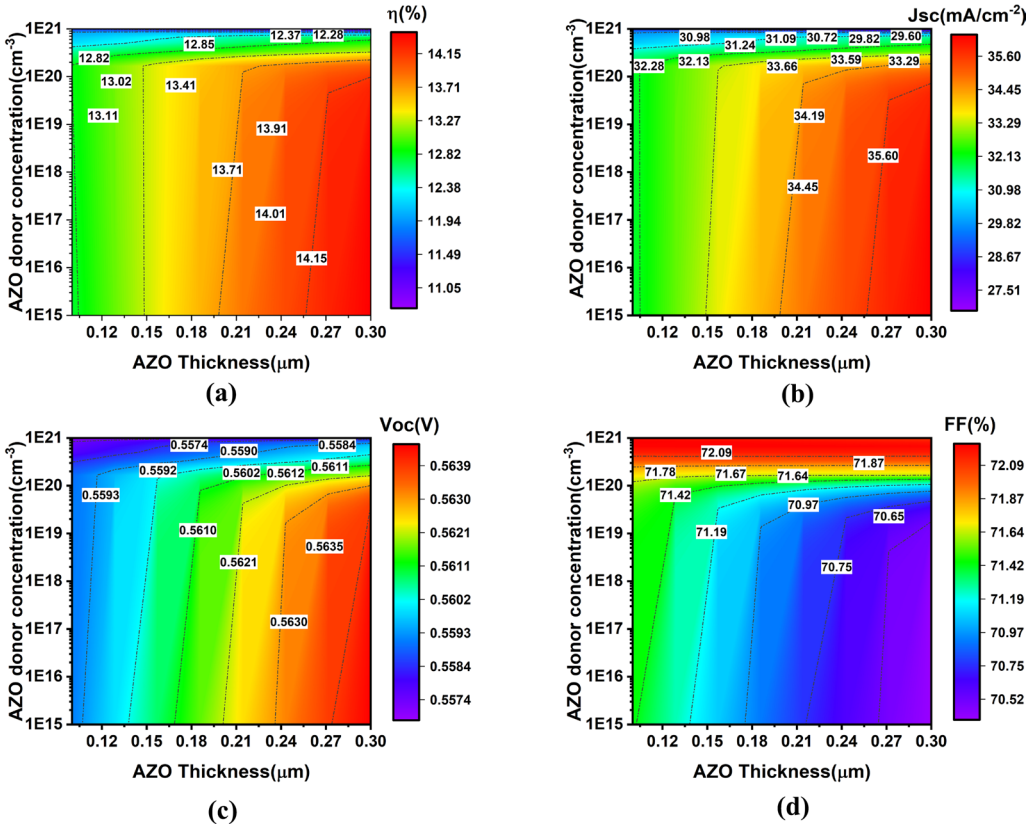

Fig. 2 2-D contour plot of solar cell performance parameters: (a) efficiency (η), (b) short circuit current density (J_{sc}), (c) open circuit voltage (V_{oc}), and (d) fill factor (*FF*) at varying AZO thickness and donor concentration.

For the concentrations of 1×10^{18}cm^{-3} and 1×10^{19}cm^{-3} , no significant improvement in efficiency has been observed, and thereafter it starts to decrease. Similar observations have been made for J_{sc}. As the area transparent to light becomes large, the collection of photogenerated carriers improves at the lower dopant concentration. Photogenerated carriers start recombining with the increase in donor concentration, which ultimately saturates the PCE, deteriorating its value for higher concentrations. J_{sc} behaves quantitatively in a similar way. However, a constant value of ~0.56 V for V_{oc} has been noted. The FF is a cumulative effect of efficiency, J_{sc} and V_{oc} , and no significant improvement has been observed at any thicknesses or dopant concentration. We obtained the optimum efficiency of 13.11% in the simulation range of the AZO layer, and 0.12-μm thickness and 1×10^{16}cm^{-3} donor concentration were the best choice for the AZO simulation parameters for the best operational efficiency.

The solar cell parameters on the contour plot for the variation of ZrS_2 thickness versus donor concentration are shown in Fig. 3. The simulation range for ZrS_2 thickness of 0.1–0.3 μm (x-axis) and donor concentration 1×10^{13}–1×10^{19}cm^{-3}(y-axis) has been considered. For any thickness value, a marginal improvement in efficiency has been observed only at high doping concentrations. If the thickness is kept constant, say at 0.18 μm, the efficiency is increased by ~3.2% and at 0.27 μm only by ~2.2%. Since J_{sc} depends particularly on the absorber layer (MoS_2) thickness, it remains constant at ~36 mAcm^{-2} for the same thickness (0.27 μm) at all doping concentrations. As the thickness of the ZrS_2 layer progresses from 0.1 to 0.3 μm, as slight increase in V_{oc} can be attributed to the accumulation of photogenerated charge carriers. The FF is the figure-of-merit of the device and depends on the series resistance. On increasing the dopant concentration, the resistance within the layer reduces, which improves the FF. For example, if we increase the doping from 1×10^{13}cm^{-3} to 1×10^{19}cm^{-3}, FF reaches 72.31% from 69.62% for ZrS_2 thickness fixed at 0.15 μm. Additionally, good conductivity and high mobility of ZrS_2 contributes towards this result.[32] The maximum efficiency of 14.69% has been estimated for extreme simulation values.

To analyze the effect of MoS_2 absorber thickness and acceptor concentration on the solar cell performance parameters, the simulation was run from 1.0 μm to 5.0 μm thickness and 1×10^{13}–1×10^{19}cm^{-3} acceptor density.

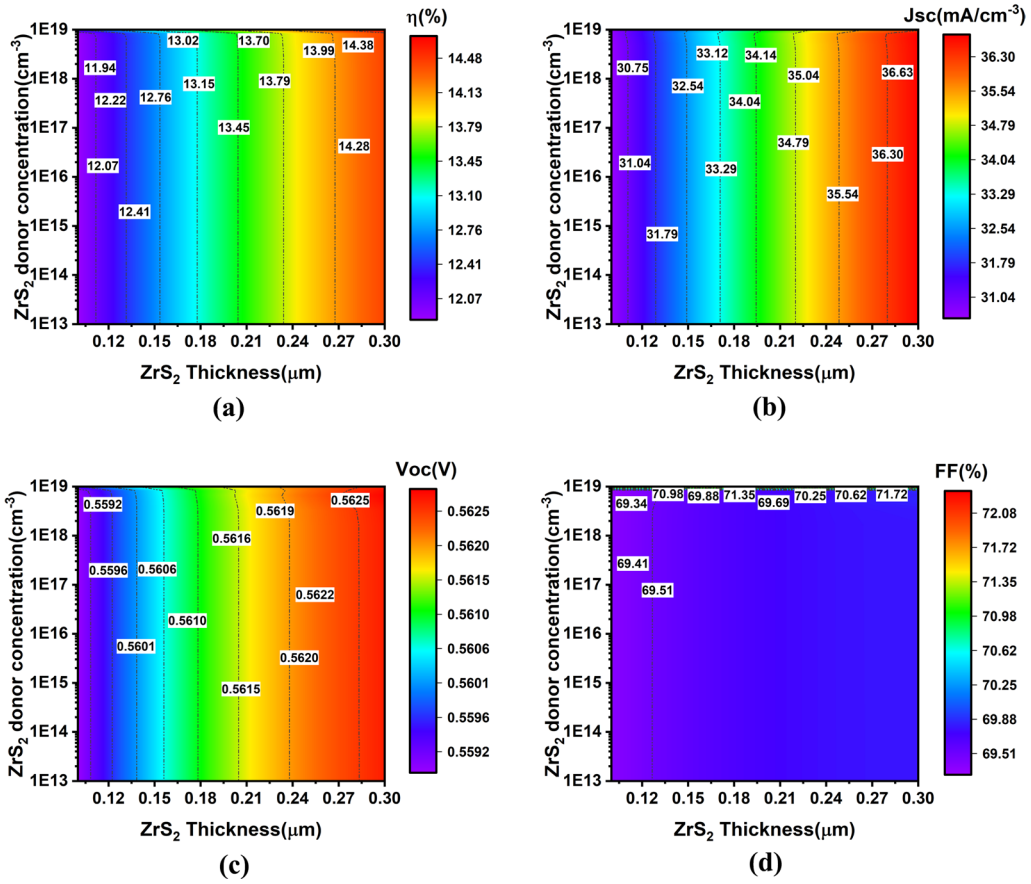

Fig. 3 2-D contour plot of solar cell performance parameters: (a) efficiency (η), (b) short circuit current density (J_{sc}), (c) open circuit voltage (V_{oc}), and (d) fill factor (FF) at varying ZrS_2 thickness and donor concentration.

The deduced parameters of efficiency, J_{sc}, V_{oc} , and FF as a function of MoS_2 thickness and doping concentration are shown in Fig. 3. Estimation of the optimum absorber thickness is the vital requirement to obtain maximum efficiency and reduce the cost of fabrication. It is observed from the contour plot that, as the thickness of the absorber layer increases, the efficiency and J_{sc} are enhanced for higher doping levels, whereas they saturates for larger thicknesses. For 1×10^{18}cm^{-3} acceptor concentration, the increase in thickness from 1.0 μm to 2.14 μm enhances the efficiency from 11.64% to 12.37%. No significant improvement in the same has been observed up to a thickness of 3.85 μm. However, at larger thicknesses, a ~1.5% increase has been observed. Simulation results of J_{sc} show a similar behavior. At a thickness of 1.0–2.14 μm, J_{sc} changes from 29.08 mAcm^{-2} to 30.57 mAcm^{-2}. The absorption at longer wavelengths improves the collection of photogenerated carriers and hence the efficiency. However, at larger thicknesses, the loss of carriers due to recombination before they reach the terminal can be attributed to a marginal enhancement of efficiency and J_{sc}. At lower doping concentrations, the efficiency reduces but J_{sc} seems to be improving. A slight improvement of V_{oc} can be noticed above the acceptor concentration of 1×10^{15}cm^{-3}. For a constant MoS_2 thickness, a change in acceptor concentration has a significant impact on the solar cell performance, as can be seen from the contour plots in Fig. 4. A high doping level enhances the number of free charge carriers, which improves the performance parameters. Nevertheless, there is a notable reduction of carriers due to recombination in extreme doping conditions that decreases the PCE. We obtained the optimum efficiency of 12.37% in the simulation range of a MoS_2 layer of 2.14 μm thickness and a 1×10^{18}cm^{-3} concentration were the best choice of the parameters for optimum efficiency.

In the next step, solar cell performance parameters were evaluated by varying the thickness of the ZrS_2 and MoS_2 layers, and the simulation results are presented in Fig. 5. Keeping the thickness of AZO fixed at 0.1 μm, the thicknesses of the ZrS_2 and MoS_2 were varied from 0.1 to 0.3 μm and from 1.0 to 5.0 μm, respectively, in five simulation steps. The efficiency change is more pronounced with the variation of ZrS_2 thickness compared to that of MoS_2 . As ZrS_2 progresses from 0.1 to 0.3 μm, PCE changes by ~17% for MoS_2 thickness fixed at 1.0 μm and by ~14% for MoS_2 thickness fixed at 5.0 μm. Efficiency loss for thicker wafers is due to the loss of mobile carriers

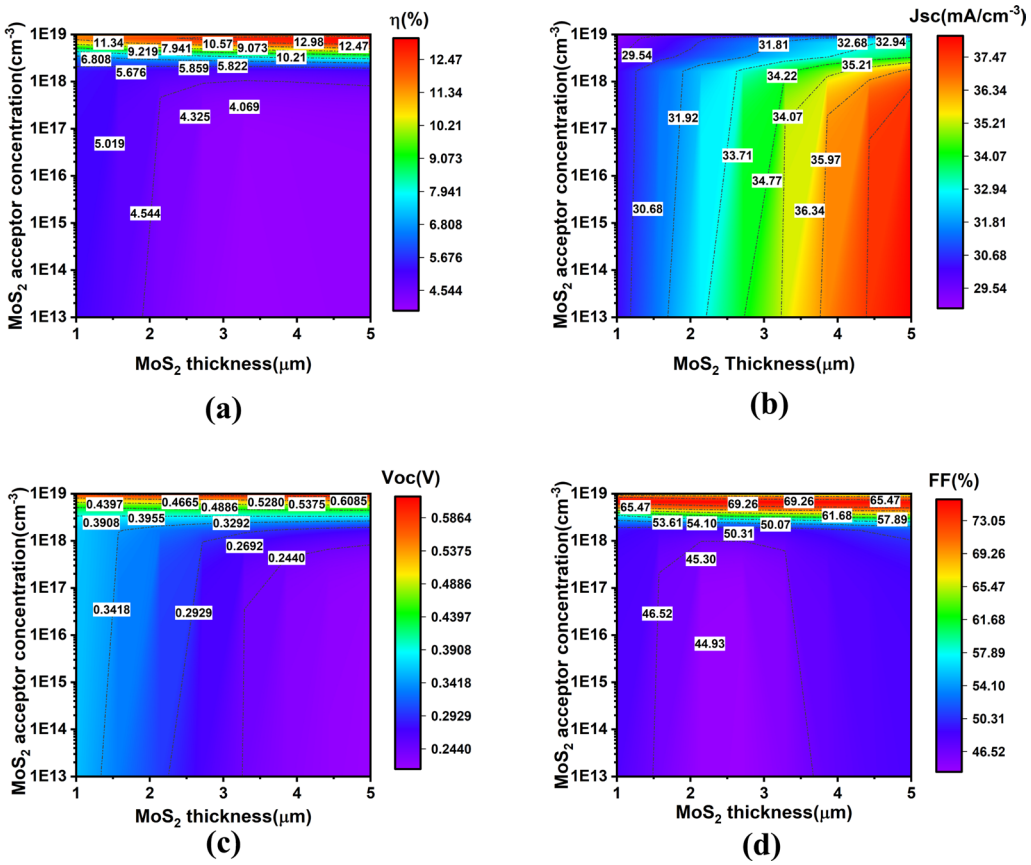

Fig. 4 2-D contour plot of solar cell performance parameters: (a) efficiency (η), (b) short circuit current density (J_{sc}), (c) open circuit voltage (V_{oc}), and (d) fill factor (FF) at varying MoS_2 thickness and donor concentration.

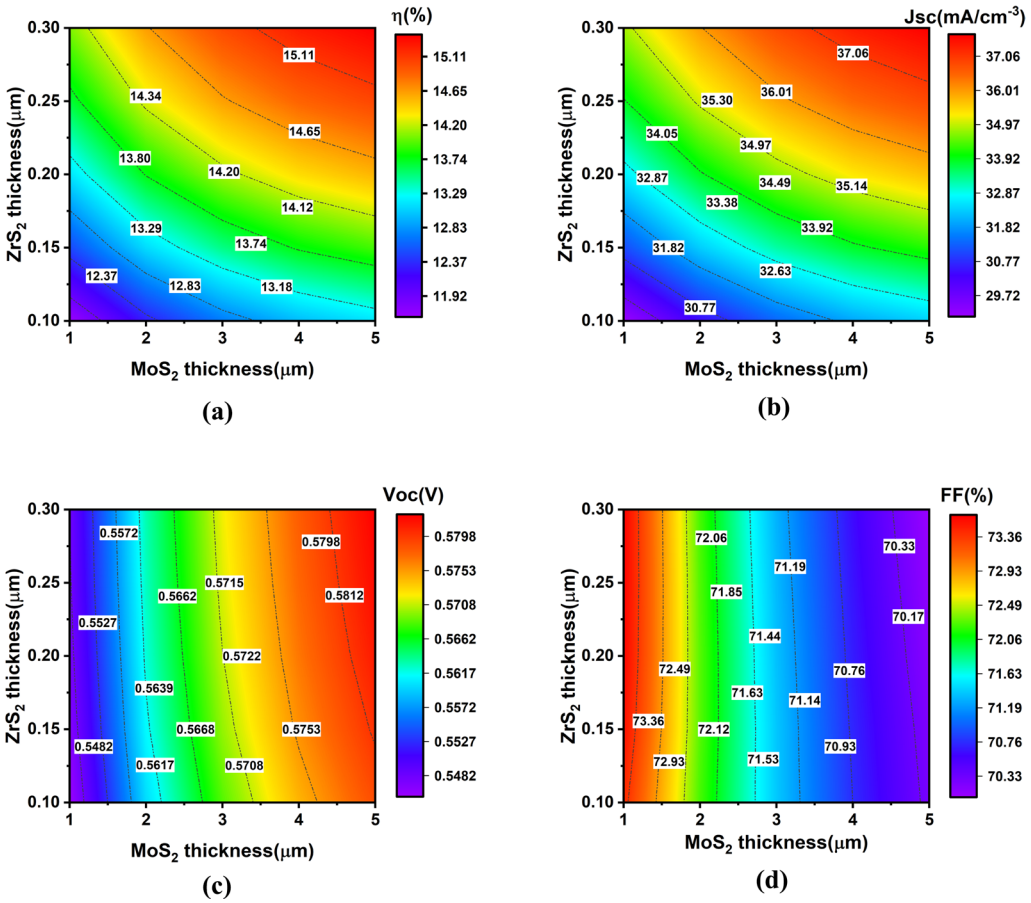

Fig. 5 2-D contour plot of solar cell performance parameters: (a) efficiency (η) (b) short circuit current density (J_{sc}), (c) open circuit voltage (V_{oc}), and (d) fill factor (*FF*) at varying ZrS_2 and MoS_2 thicknesses.

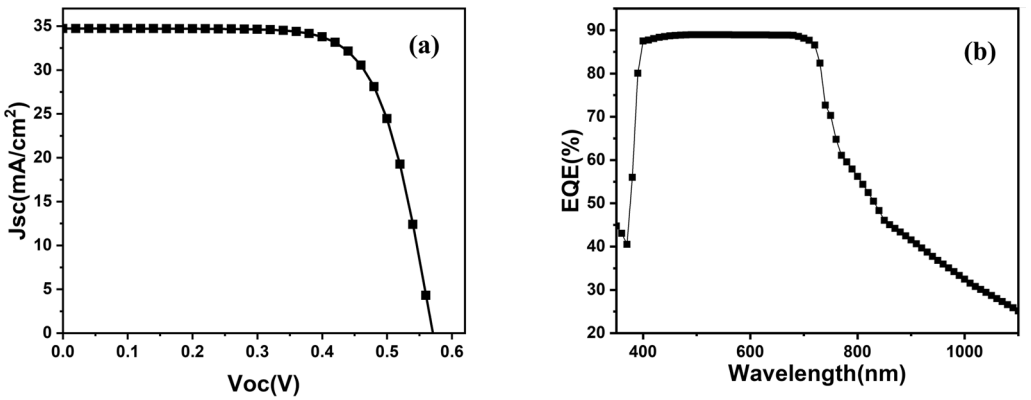

Fig. 6 (a) *J–V* characteristics and (b) EQE response curve of ZrS_2/MoS_2 solar cell.

to recombination before reaching the back contact. Since the charge carriers reduce, J_{sc} is also affected similarly, as can be seen from the graph. It is interesting to note that ZrS_2 thickness variation has a negligible effect on FF, whereas MoS_2 produces a noticeable change in FF. Good conductivity, high mobility, and the intrinsically *n*-type characteristic of ZrS_2 material leads to low series resistance and hence no change in FF. At ZrS_2 and MoS_2 thicknesses of 0.2 μm and 3.0 μm, respectively, the estimated PCE = 14.13%, J_{sc} = 34.72 mAcm^{-2}, V_{oc} = 0.5707 V, and

FF = 71.35% are the optimal values under the simulation conditions. The results obtained are comparable to those of the CdTe/MoS_2 structure with an efficiency of 13.7% [33], whereas Haque et al. calculated an efficiency of 21% for the Al-FTO/n-CdS/p-MoS_2 structure.[34]

The *J–V* characteristics and EQE response of the ZrS_2/MoS_2 heterojunction at optimized simulation parameters are shown in Fig. 6(a, b). As can be seen from the plots, the modeled heterojunction has been found to be appropriate for solar power conversion in the visible region of the electromagnetic spectrum.

Effect of Different Metal Work Function

The work function of metal contacts plays an important role in determining the overall performance of a device.[35,36] In this study, the solar cell parameters have been estimated with aluminum as metal front contact and molybdenum as the metal back contact. In order to investigate the influence of work function on solar cell parameters, three metals, gold (Au), nickel (Ni), and platinum (Pt) were considered for the back contact. With these metal back contacts and an aluminum front contact, the *J–V* parameters have been calculated, as presented in Table II. A maximum efficiency of 24.3% has been confirmed with the Pt back contact. With the Ni back contact, the value remains almost the same; however, a drop of ~40% has been observed with the Au back contact. The phenomenon of improving solar cell efficiency with an increase in metal work function can be attributed to the decrease of Schottky barrier height at the back contact, which ultimately improves the flow of the generated charge carriers.

Table II *J–V* parameters for different metal back contacts

Metal work function, eV [37]	V_{oc}, Volts	J_{sc}, mA/cm^2	FF, %	PCE, %
5.1, Au	0.6707	34.73	74.5	17.35
5.5, Ni	0.8524	34.76	81.73	24.2
5.7, Pt	0.8528	34.89	81.72	24.3

Effect of Defect Density

A neutral defect density defines the charge carrier diffusion length and lifetime in the material. Solar cell performance is adversely affected by increasing the defect density. In order to study the influence of increasing defects on solar cell performance parameters, the defect density in the ZrS_2 and MoS_2 layers have been separately varied in the range 1×10^{13}–1×10^{17}cm^{-3}, and the simulation results are presented in Fig. 7. Figure 7a shows the impact of varying the defect density in ZrS_2 on solar cell performance parameters. The photogenerated carriers are lost to the recombination process as defects in the material increase. This automatically deteriorates the PCE of the solar cell. However, the good

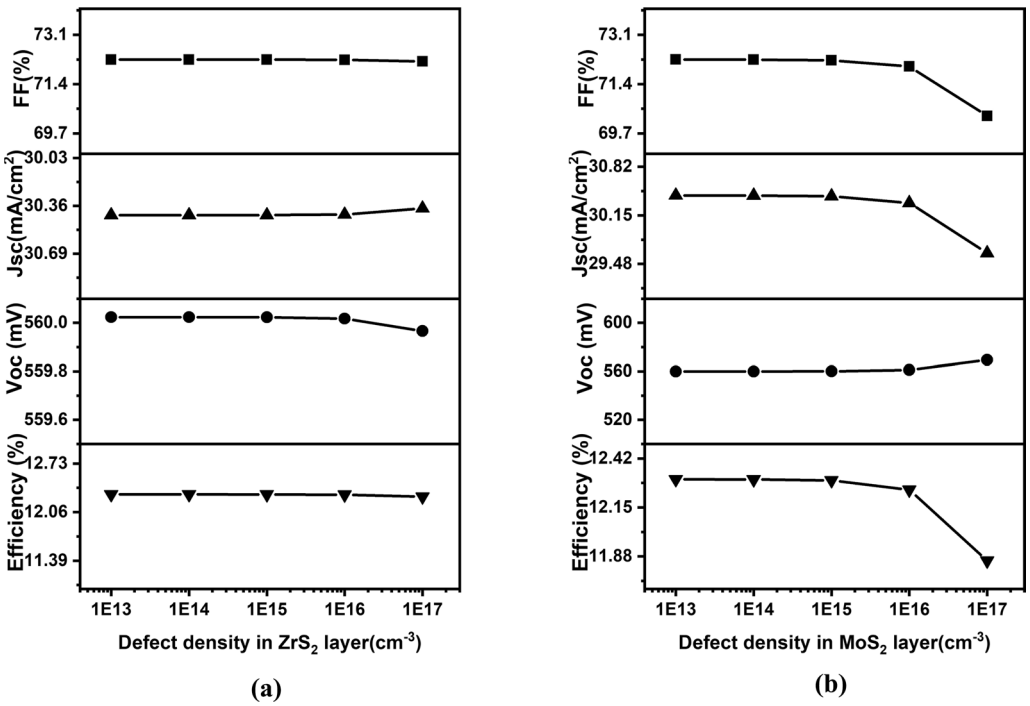

Fig. 7 Solar cell performance parameters versus defect density in (a) the ZrS_2 layer and (b) the MoS_2 layer.

conductivity, high electron mobility, and high carrier concentration of ZrS_2 layer have negligible effects on the solar cell performance. A ~0.24% change in efficiency has been noticed when the defects increase by 10-fold from 1×10^{16}cm^{-3}. The defects in MoS_2 layer were varied, keeping the defects in ZrS_2 fixed at 1×10^{14}cm^{-3}. For a neutral defect density level up to 1×10^{16}cm^{-3} , the change in the performance is not distinguishable. The free carriers outnumber the defects in the MoS_2 layer, which do not influence the device performance. However, the device performance is degraded when the defect density is increased to 1×10^{17}cm^{-3}. The PCE was reduced by ~3.2% and other parameters have a similar effect.

Effect of Absorber Layer Grading

The efficiency of the modeled ZrS_2/MoS_2 heterostructure can be improved by using a graded profile of the MoS_2 layer. The SCAPS tool supports the numerical simulation of a graded structure by modifying the transport equations with position-dependent electron affinity (χ), a mobility gap (E_G), and the density of states at the conduction band edge (N_c) and the valence band edge (N_v), as:

$$J_n = -q\mu_n n\frac{dV}{dx} - q\mu_n n\frac{d\chi}{dx} + qD_n\frac{dn}{dx} + qD_n n\frac{d\ln(N_c)}{dx} \quad (4)$$

$$J_p = -q\mu_p p\frac{dV}{dx} - q\mu_p p\frac{d(\chi + E_G)}{dx} - qD_p\frac{dp}{dx} + qD_p p\frac{d\ln(N_v)}{dx} \quad (5)$$

where μ_n is the electron mobility, D_n is the electron diffusion coefficient, and μ_p and D_p are similarly defined for holes. Compositional grading of the constituent elements in the semiconductor layer is governed by several grading laws, as defined in SCAPS.[28] The graded compound is assumed to be of composition $A_{1-y}B_y$, where materials A ($y = 0$) and B ($y = 1$) are defined with the respective pure layer properties. The composition value, y, has been set from left to right. The grading law, as described in SCAPS, is implemented along the thickness of the layer under consideration. This is the material-driven approach utilized by SCAPS to evaluate P{$y(x)$}, where P represents a material parameter. In our simulation model. the exponential grading law (Eq. 6) has been implemented to enhance the efficiency of the optimized ZrS_2/MoS_2 heterostructure:

$$y(x) = P_0 + (P_A - P_0)\frac{\sinh\left(\frac{y_B - y}{L_A}\right)}{\sinh\left(\frac{y_B - y_A}{L_A}\right)} + (P_B - P_0)\frac{\sinh\left(\frac{y - y_B}{L_B}\right)}{\sinh\left(\frac{y_B - y_A}{L_B}\right)} \quad (6)$$

where P_0 is the background bulk concentration value, L_A and L_B are the characteristic lengths, and subscripts A and B represent the pure materials MoS_2 and $MoSe_2$, respectively.

The optimized efficiency of 14.13% has been obtained for the ZrS_2/MoS_2 heterostructure as discussed above. Now, the conversion efficiency has been improved by selenization of the absorber layer (MoS_2). Selenization tailors the band gap of the graded compound between the band gap energy of MoS_2 and $MoSe_2$,i.e., 1.29–1.4 eV. Figure 8 shows the PCE of the $ZrS_2/Mo(S_xSe_{1-x})_2$ junction for the variation of left and right composition in the range 0.1–0.9 along the thickness of the material. It can be inferred from the plot that an increase in selenium concentration has a favorable effect on the generation of charge carriers. The PCE increases as the selenium concentration increases. At the simulation extremes, an efficiency up to 21.14% has been achieved.

Conclusions

The SCAPS-based simulation model of an AZO/ZrS_2/MoS_2 heterojunction has been proposed and optimized for efficient photovoltaic response. The performance parameters of the heterojunction have been carefully investigated by varying the thickness of the constituent layers and respective doping concentrations. For the optimal thickness values of 0.1 μm, 0.2 μm, and 3.0 μm of the AZO, ZrS_2 , and MoS_2 layers, respectively, the highest efficiency of 14.13% has been evaluated with the other parameters of0 $V_{oc} = 0.5707$ V, $J_{sc} = 34.02$ mA/cm^3 , and FF = 71.35%. The external quantum efficiency response illustrates the absorption in the visible region of the electromagnetic spectrum. Furthermore, the efficiency improvement has been studied by the selenization of the MoS_2 absorber layer using the exponential grading law in SCAPS. An efficiency of 21.14% has been achieved for the maximum simulation range considered. Therefore, a heterojunction between transition metal chalcogenides can

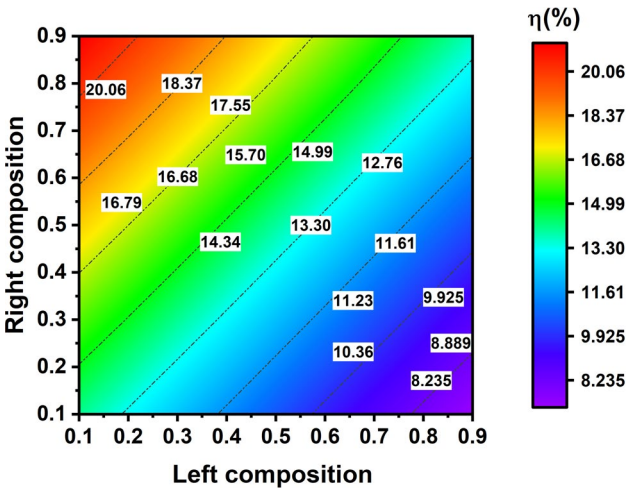

Fig. 8 The obtained efficiency versus left composition and right composition for the ZrS_2/MoS_2 structure.

be beneficial for photovoltaic applications compared to Cd-based materials.

Acknowledgments The authors wish to thank Dr. M. Burgelman's group of Electronics and Information Systems (ELIS) University of Gent for the SCAPS-1D program tool.

Data Availability The data that supports the findings of this study are available openly and the cited references have been mentioned within this article.

Conflict of interest On behalf of all authors, the corresponding author states that there is no conflict of interest.

References

1. J.O. Island, A.J. Molina-Mendoza, M. Barawi, R. Biele, E. Flores, J.M. Clamagirand, J.R. Ares, C. Sánchez, H.S. Van Der Zant, R. Dagosta, and I.J. Ferrer, Electronics and optoelectronics of quasi-1D layered transition metal trichalcogenides. *2D Materials.* 4(2), 022003 (2017).
2. Y. Cui, Z. Zhou, T. Li, K. Wang, J. Li, and Z. Wei, Versatile crystal structures and (opto)electronic applications of the 2D metal mono- Di-, and Tri-Chalcogenide Nanosheets. *Adv. Funct. Mater.* 29, 1900040 (2019).
3. P. Chandra and M. Shaikh, Nanomaterials via Single-Source Precursors: Synthesis, Processing and Applications ed. by A.W. Apblett, A.R. Barron, A.F. Hepp(Elsevier, Netherlands, 2022) p. 389.
4. S. Palchoudhury, K. Ramasamy, J. Han, P. Chen, and A. Gupta, Transition metal chalcogenides for next-generation energy storage. *Nanoscale Adv.* 5, 2724 (2023).
5. S.E. Sheela, R. Sekar, D.K. Maurya, M. Paulraj, and S. Angaiah, Progress in transition metal chalcogenides-based counter electrode materials for dye-sensitized solar cells. *Mater. Sci. Semicond. Process.* 156, 107273 (2023).
6. O. Öztürk, and E. Gür, Layered transition metal sulfides for supercapacitor applications. *ChemElectroChem* (2024). https://doi.org/10.1002/celc.202300575.
7. S. Joseph, J. Mohan, S. Lakshmy, S. Thomas, B. Chakraborty, S. Thomas, and N. Kalarikkal, A review of the synthesis, properties, and applications of 2D transition metal dichalcogenides and their heterostructures. *Mater. Chem. Phys.* 297, 127332 (2023).
8. S. Gupta, G. Shishodia, and P.K. Shishodia, A comparative study of ZrS2-based thin film solar cells using the SCAPS solar cell capacitance simulator. *Semicond. Sci. Technol.* 38, 025012 (2023).
9. L. Li, H. Wang, X. Fang, T. Zhai, Y. Bando, and D. Golberg, High-performance schottky solar cells using ZrS2 nanobelt networks. *Energy Environ. Sci.* 4, 2586 (2011).
10. P.P. Sanap, S.P. Gupta, S.S. Kahandal, J.L. Gunjakar, C.D. Lokhande, B.R. Sankapal, Z. Said, R.N. Bulakhe, J. Man Kim, and A.B. Bhalerao, Exploring vanadium-chalcogenides toward solar cell application: a review. *J. Ind. Eng. Chem.* 129, 124 (2024).
11. A. Raj, M. Kumar, D.V. Singh, and A. Anshul, A critical review on transition metal dichalcogenides (TMDs): an efficiency booster for perovskite solar cells. *FlatChem* 44, 100629 (2024).
12. Y. Tian, Y. Cheng, J. Huang, S. Zhang, H. Dong, G. Wang, J. Chen, J. Wu, Z. Yin, and X. Zhang, Epitaxial growth of large area ZrS2 2D semiconductor films on sapphire for optoelectronics. *Nano Res.* 15, 6628 (2022).
13. M. Mattinen, G. Popov, M. Vehkamäki, P.J. King, K. Mizohata, P. Jalkanen, J. Räisänen, M. Leskelä, and M. Ritala, Atomic layer deposition of emerging 2D semiconductors, HfS2 and ZrS2, for optoelectronics. *Chem. Mater.* 31, 5713 (2019).
14. X. Wang, L. Tong, W. Fan, W. Yan, C. Su, D. Wang, Q. Wang, H. Yan, and S. Yin, Air-stable self-powered photodetector based on TaSe2/WS2/TaSe2 asymmetric heterojunction with surface self-passivation. *J. Colloid Interface Sci.* 657, 529 (2024).
15. J. Sun, Z. Lin, X. Jia, H. Li, C. Song, F. Pan, L. Fang, J. Zhang, and Y. Wang, High-performance 2D WS2 photodetector enhanced by charge-transfer doping through NH3 annealing. *Mater. Today Phys.* 35, 101133 (2023).
16. Q. Wu, C. Wang, L. Li, X. Zhang, Y. Jiang, Z. Cai, L. Lin, Z. Ni, X. Gu, K. Ostrikov, H. Nan, and S. Xiao, Fast and broadband MoS2 photodetectors by coupling WO3–x semi-metal nanoparticles underneath. *J. Mater. Sci. Technol.* (2024). https://doi.org/10.1016/j.jmst.2023.12.059.
17. N. Roy, Design and performance evaluation of MoS2 photodetector in vertical MSM configuration. *Opt. Mater. Amst* 148, 114817 (2024).
18. M. Hamada, K. Matsuura, T. Hamada, I. Muneta, K. Kakushima, K. Tsutsui, and H. Wakabayashi, ZrS2 symmetrical-ambipolar FETs with near-Midgap TiN film for both top-gate electrode and schottky-barrier contact. *Jpn. J. Appl. Phys.* 60, SBBH05 (2021).
19. A. Nourbakhsh, A. Zubair, R.N. Sajjad, K.G.A. Tavakkoli, W. Chen, S. Fang, X. Ling, J. Kong, M.S. Dresselhaus, E. Kaxiras, and K.K. Berggren, MoS2 field-effect transistor with sub-10 Nm channel length. *Nano Lett.* 16(12), 7798 (2016).
20. M.W. Iqbal, M. Manzoor, A. Islam, N.A. Noor, S. Aftab, A.U. Rahman, and T. Zahid, The effect of DUV-O2 doping on WSe2 FET for sensing applications: experimental and theoretical approach. *Micro Nanostruct.* 163, 107127 (2022).
21. M.T.L. Lai, K.M. Lee, T.C.K. Yang, G.T. Pan, C.W. Lai, C.Y. Chen, M.R. Johan, and J.C. Juan, The improved photocatalytic activity of highly expanded MoS2 under visible light emitting diodes. *Nanoscale Adv* 3, 1106 (2021).
22. C. Liu, Y. Lu, X. Yu, R. Shen, Z. Wu, Z. Yang, Y. Yan, L. Feng, and S. Lin, Hot carriers assisted mixed-dimensional graphene/MoS2/p-GaN light emitting diode. *Carbon NY* 197, 192 (2022).
23. C. Yan, C. Gong, P. Wangyang, J. Chu, K. Hu, C. Li, X. Wang, X. Du, T. Zhai, Y. Li, and J. Xiong, 2D group IVB transition metal dichalcogenides. *Adv. Funct. Mater.* 28, 1803305 (2018).
24. S. Gupta, G. Shishodia, and P.K. Shishodia, Computational analysis to study the effect of selenization on ZrS2/CZTS heterostructure performance. *Eng. Res. Express* 4, 035026 (2022).
25. R. Chaudhary, K. Patel, R.K. Sinha, S. Kumar, and P.K. Tyagi, Potential application of mono/Bi-layer molybdenum disulfide (MoS2) sheet as an efficient transparent conducting electrode in silicon heterojunction solar cells. *J. Appl. Phys.* 120, 013104 (2016).
26. R. Singh, A. Giri, M. Pal, K. Thiyagarajan, J. Kwak, J.J. Lee, U. Jeong, and K. Cho, Perovskite solar cells with an MoS2 electron transport layer. *J. Mater. Chem. A Mater.* 7, 7151 (2019).
27. S. Gupta, G. Shishodia, and P. K. Shishodia in *Recent Advances in Nanotechnology: ICNOC 2022, Springer Proceedings in Materials*(2023) p. 163.
28. M. Burgelman, K. Decock, A. Niemegeers, J. Verschraegen, and S. Degrave, SCAPS Manual https://scaps.elis.ugent.be/SCAPS%20manual%20most%20recent.pdf. Accessed 20 September 2023.
29. S.M.Sze, SEMICONDUCTOR DEVICES: PHYSICS AND TECHNOLOGY, 2nd edn. (John Wiley and Sons, INC. 2008).
30. H. Movla, Optimization of the CIGS based thin film solar cells: numerical simulation and analysis. *Optik* 125(1), 67 (2014).
31. M.D. Haque, M.H. Ali, M.F. Rahman, and A.Z. Islam, Numerical analysis for the efficiency enhancement of MoS2 solar cell: a

simulation approach by SCAPS-1D. *Opt. Mater.* 1(131), 112678 (2022).
32. M. Hamada, K. Matsuura, T. Sakamoto, I. Muneta, T. Hoshii, K. Kakushima, K. Tsutsui, and H. Wakabayashi, High hall-effect mobility of large-area atomic-layered polycrystalline ZrS2 film using UHV RF magnetron sputtering and sulfurization. *IEEE J. Electron. Dev. Soc.* 7, 1258 (2019).
33. S. Yuan, M.J. Zhang, X. Yang, Z. Mei, Y. Chen, and F. Pan, A novel MoS2-based hybrid film as the back electrode for high-performance thin film solar cells. *RSC Adv.* 7, 23415 (2017).
34. D. Haque, H. Ali, F. Rahman, and A.Z.T. Islam, Numerical analysis for the efficiency enhancement of MoS2 solar cell: a simulation approach by SCAPS-1D. *Opt. Mater.* 131, 112678 (2022).
35. F.Z. Boutebakh, M.L. Zeggar, N. Attaf, and M.S. Aida, Electrical properties and back contact study of CZTS/ZnS heterojunction. *Optik* 1(144), 180 (2017).
36. J.J. Scragg, J.T. Wätjen, M. Edoff, T. Ericson, T. Kubart, and C. Platzer-Björkman, A detrimental reaction at the molybdenum back contact in Cu 2ZnSn(S, Se)4 thin-film solar cells. *J. Am. Chem. Soc.* 134, 19330 (2012).
37. P. Sawicka-Chudy, Z. Starowicz, G. Wisz, R. Yavorskyi, Z. Zapukhlyak, M. Bester, M.S. GLowa, and M. Cholewa, Simulation of TiO2/CuO solar cells with SCAPS-1D software. *Mater. Res. Express* 6, 085918 (2019).